

Informative Goodness-of-Fit for Multivariate Distributions

Sara Algeri¹

¹ School of Statistics, University of Minnesota,
0461 Church St SE, Minneapolis, MN 55455, USA.

Email: salgeri@umn.edu

Abstract

This article introduces an informative goodness-of-fit (iGOF) approach to study multivariate distributions. When the null model is rejected, iGOF allows us to identify the underlying sources of mismodeling and naturally equips practitioners with additional insights on the nature of the deviations from the true distribution. The informative character of the procedure is achieved by exploiting smooth tests and random fields theory to facilitate the analysis of multivariate data. Simulation studies show that iGOF enjoys high power for different types of alternatives. The methods presented here directly address the problem of background mismodeling arising in physics and astronomy. It is in these areas that the motivation of this work is rooted.

Multivariate goodness-of-fit, Rosenblatt transform, smooth tests, background mismodeling.

1 Introduction

Scientific motivations. When searching for the signals of new particles, or when aiming to detect new astronomical objects, a common difficulty arising in the analysis of the data collected by the detectors is the impossibility of correctly specifying the background distribution. In physics and astronomy, we typically refer with “background” or “noise” to the signal of all the astrophysical sources which are not those we aim to discover. Unfortunately, since many sources contribute to the background, its distribution is particularly difficult to model (e.g., [Priel et al., 2017](#); [Dauncey et al., 2015](#); [Algeri et al., 2018](#)).

Moreover, if the model postulated by the scientists is rejected, it is often difficult to identify the invalidating causes. As a result, this aspect is typically addressed by conducting a suite of exploratory analyses to adequately constrain the parameters involved, followed by a validity check for a newly postulated distribution. Given the complexity of the models investigated through physics experiments, however, this may result in a substantial investment of resources (e.g., [Balázs et al., 2017](#)); even more so when having to choose between tens of plausible theoretical models (e.g., [Scott, 2018](#)).

Statistical formulation of the problem. In statistical terms, these difficulties translate into two main questions arising in the statistical analysis of multivariate data. Specifically, given a random vector $\mathbf{X} = (X_1, \dots, X_p)$, we may wonder:

- Q1. *is the distribution of \mathbf{X} correctly specified and, if not, in what way the true data distribution diverges from that hypothesized under the null hypothesis?*
- Q2. *How can we improve our postulated model? Or in other words, can we provide a data-driven correction of for it?*

As noted by [Pearson \(1938\)](#), smooth tests, originally introduced by [Neyman \(1937\)](#), naturally allow us to capture and model the departure of f from g and thus, they offer the framework to directly address Q1 and Q2.

In order to provide a high level overview on smooth tests, let f be the true (unknown) probability density function (pdf) of a random variable $X \in \mathbb{R}$, g is the hypothesized density and G the respective cumulative density function (cdf). For example, in the above-mentioned problem of background mismodeling, f represents the true background distribution and g is the background model postulated by the scientists. A smooth model for the true probability law f can be specified as

$$f(x) = g(x)d(G(x)) = g(x) \left\{ 1 + \sum_{j \geq 1} \theta_j T_j[G(x)] \right\}, \quad (1)$$

where $d(G(x)) = \frac{f(x)}{g(x)}$ is the likelihood ratio and the term in the curly brackets is an orthonormal expansion for d . A smooth test (e.g., [Neyman, 1937](#); [Barton, 1953](#); [Ledwina, 1994](#)) consists of testing if any of the coefficients θ_j in (1) is different from zero. Finally, by estimating $d(G(x))$ and constructing adequate confidence bands, it is possible to visualize the nature of the departure of f from g .

Despite their usefulness, smooth tests are mainly limited to the univariate setting. In light of this, the main methodological task of this work is to extend this framework to allow for the analysis of multivariate data.

Main results and organization. The theoretical framework is presented in Section 2. There, we define a suitable expansion of the likelihood ratio through orthonormal functions on the unit cube. As shown in Sections 3 and 4, such representation substantially simplifies the subsequent stages of estimation, model selection and (post-selection) inference. In Section 5, we discuss a simple ANOVA-like testing strategy to identify possible sources of misspecification. Power studies are conducted via simulations in both Sections 4 and 5. As noted above, this work finds its main motivations in the context of astrophysical searches. Therefore, in Section 6 we illustrate how iGOF can be used to address the problem of misspecification of the cosmic background considering a realistic simulation from the Fermi Large Area Telescope ([Atwood et al., 2009](#)). Despite this article mainly focuses on the analysis of continuous data, extensions to the discrete setting are discussed in Section 7. Section 8 collects a summary of the results and a discussion of the limitations of iGOF. Technical proofs and codes are provided in the Supplementary Material. A summary of the main notation used throughout the paper is available in the Appendix.

2 Theoretical framework

2.1 Transformations of the likelihood ratio on the unit cube

Suppose F is the true distribution function of a random vector $\mathbf{X} \in \mathcal{X} \subseteq \mathbb{R}^p$ and denote with G its hypothesized distribution. F and G are assumed to be continuous with densities f and g . Furthermore, assume that $f(\mathbf{x}) = 0$ whenever $g(\mathbf{x}) = 0$. For every $\mathbf{x} = (x_1, \dots, x_p) \in \mathcal{X}$, the hypothesized density g is such that

$$g(\mathbf{x}) = \prod_{d=1}^p g_d(x_d | \mathbf{x}_{<d}),$$

where $\mathbf{x}_{<d} = (x_1, \dots, x_{d-1})$ and g_1, \dots, g_p are suitable densities with associated cdfs and quantile functions G_d and Q_d , for all $d = 1, \dots, p$. The likelihood ratio between F and G can be specified as

$$d(\mathbf{u}) = \frac{f(\mathbf{Q}(\mathbf{u}))}{g(\mathbf{Q}(\mathbf{u}))}, \quad \mathbf{u} \in [0, 1]^p \quad (2)$$

where $\mathbf{u} = (u_1, \dots, u_p) = (G_1(x_1), \dots, G_p(x_p | \mathbf{x}_{<p})) = \mathbf{G}_R(\mathbf{x})$ is the Rosenblatt transformation (Rosenblatt, 1952)¹. Whereas, $\mathbf{Q}(\mathbf{u}) = (Q_1(u_1), \dots, Q_p(u_p))$, for all $d = 1, \dots, p$.

In the bivariate setting, for instance, let $G_1 \equiv G_{X_1}$ and $G_2 \equiv G_{X_2|X_1}$, i.e., the hypothesized marginal cdf of X_1 and the hypothesized conditional cdf of $X_2|X_1$, respectively. Hence, (2) specifies as

$$d(u_1, u_2) = \frac{f_{X_1 X_2}(Q_1(u_1), Q_2(u_2))}{g_{X_1 X_2}(Q_1(u_1), Q_2(u_2))}.$$

Remark 2.1. *As a plausible alternative to Rosenblatt's transform, one could choose each $G_d \equiv G_{X_d}$, which corresponds to assuming independence among the components of \mathbf{X} . In this setting, (2) is the copula density (e.g., Nelsen, 2007) of \mathbf{X} under G . Despite this choice could simplify substantially the computations, it would not allow to test models*

¹Notice that, in general, $\mathbf{G}_R(\mathbf{x}) \neq G(\mathbf{x})$ as the Rosenblatt's transform $\mathbf{G}_R(\mathbf{x}) \in [0, 1]^d$ whereas the cdf $G(\mathbf{x}) \in [0, 1]$.

where the components of \mathbf{X} are assumed to be dependent. Moreover, it is worth pointing out that there are situations where such transformation cannot be specified (e.g., Section 6).

To provide a sufficiently detailed representation of the substructures characterizing the distribution of \mathbf{X} (see Q1 in Section 1), a natural approach is that of expressing (2) by means of a suitable orthonormal basis in $L^2[0, 1]^p$.

For instance, let $T_{j_d}(u_d)$ be the j_d^{th} normalized shifted Legendre polynomial evaluated at $u_d = G_d(x_d | \mathbf{x}_{<d})$, with $T_0(u_d) = 1$, $T_1(u_d) = \sqrt{12}(u_d - 0.5)$, etc. (e.g., Section ??, Supplementary Material). Each $\{T_{j_d}(u_d)\}_{j_d \geq 0}$ forms a basis in $L^2[0, 1]$. Hence, we can exploit a well known result in Hilbert space theory (e.g., Proposition 2 Reed and Simon, 1980, p.50) which asserts that given two orthonormal bases $\{\psi_j\}$, $\{\phi_k\}$ for the Hilbert spaces \mathcal{H}_1 , \mathcal{H}_2 , then $\{\psi_j \otimes \phi_k\}$ is an orthonormal basis for $\mathcal{H}_1 \otimes \mathcal{H}_2$. It follows that the tensor product basis $\{T_{j_1, \dots, j_p}(\mathbf{u})\}_{j_1 \dots j_p \geq 0}$ of functions

$$T_{j_1 \dots j_p}(\mathbf{u}) = \prod_{d=1}^p T_{j_d}(u_d) \quad (3)$$

forms an orthonormal basis on $L^2[0, 1]^p$, the Hilbert space of square integrable function over the p -dimensional unit cube.

Notice that despite any orthonormal basis in $[0, 1]$ could be used to construct a tensor product basis in $[0, 1]^p$, here we focus on the normalized shifted Legendre polynomials. This choice is justified by the fact that the latter are special cases of the so called LP-score functions (Mukhopadhyay and Wang, 2020, e.g.). As discussed in Section 7, the LP score functions allow for extensions to the discrete setting.

Finally, under the assumption $d(\mathbf{u}) \in L^2[0, 1]^p$, we can write

$$d(\mathbf{u}) = \sum_{j_1 \geq 0, \dots, j_p \geq 0} \theta_{j_1 \dots j_p} T_{j_1 \dots j_p}(\mathbf{u}), \quad \mathbf{u} \in [0, 1]^p \quad (4)$$

with $\theta_{j_1 \dots j_p} = \int_{[0,1]^p} T_{j_1 \dots j_p}(\mathbf{u}) d(\mathbf{u}) d\mathbf{u}$. The expansion in (4) follows from Theorem II.6 in [Reed and Simon \(1980\)](#) and it is equivalent to say that the sum on the right-hand side converges to $d(\mathbf{u})$ in $L^2[0,1]^p$.

Remark 2.2. *An anonymous referee correctly pointed out that the likelihood ratio can also be expanded through an orthonormal expansion on the original domain \mathcal{X} , bypassing the need of Rosenblatt’s transform. In our context, however, the Rosenblatt transform is particularly useful for two main reasons. First of all, one can show (Proposition 3.1 to follow) that $d(\mathbf{u})$ corresponds to the density of $\mathbf{U} = \mathbf{G}_R(\mathbf{X})$. This fact will simplify substantially the estimation process (Section 3). Second, by transforming the data on the compact domain $[0,1]^p$ we will be able to exploit results from random fields theory to perform inference (Section 4).*

3 Estimation

The summations in (4) are taken up to infinity. However, to make the expansion operational, it is necessary to truncate the series in (4) at integers values m_1, \dots, m_p . That is because, effectively, the coefficients $\theta_{j_1 \dots j_p}$ need to be estimated and, consequently, the more terms are included in (4), the larger the variance of the resulting estimator of $d(\mathbf{u})$ (see Section 4.2 for a more detailed discussion on model selection).

For the sake of simplifying the notation in this section and those to follow, denote with \mathcal{K} the set

$$\mathcal{K} := \left\{ \{j_1 \dots j_p\}, \text{ with } j_d = 0, \dots, m_d, \text{ for all } d = 1, \dots, p, \text{ and } \sum_{d=1}^p j_d \neq 0 \right\} \quad (5)$$

of cardinality $|\mathcal{K}| = M = \prod_{d=1}^p (m_d + 1) - 1$. That is, \mathcal{K} contains all the p -tuples $\{j_1 \dots j_p\}$ of indexes $j_d = 0, \dots, m_d$, $d = 1, \dots, p$ apart from the p -tuple $\{0 \dots 0\}$. Let $\boldsymbol{\theta}$ be the $M \times 1$ vector of components θ_k , with $k \in \mathcal{K}$. Similarly, denote with $\mathbf{T}(\mathbf{u})$ the $M \times 1$ vector of elements $T_k(\mathbf{u})$, $k \in \mathcal{K}$.

Consider $\mathbf{x}_1, \dots, \mathbf{x}_n$, a sample of n i.i.d. observations from \mathbf{X} , and let $\mathbf{U} = \mathbf{G}_R(\mathbf{X})$ be the respective Rosenblatt transformation. Denote with $\mathbf{u}_1, \dots, \mathbf{u}_n$ the sample of elements $\mathbf{u}_i = \mathbf{G}_R(\mathbf{x}_i)$. The parameter $\boldsymbol{\theta}$ can be estimated by means of the vector $\hat{\boldsymbol{\theta}}$ of components

$$\hat{\theta}_k = \frac{1}{n} \sum_{i=1}^n T_k(\mathbf{u}_i) \quad \text{for all } k \in \mathcal{K}, \quad (6)$$

The mean and covariance matrix of $\hat{\boldsymbol{\theta}}$ and an estimator of $d(\mathbf{u})$ are given in Proposition 3.1.

Proposition 3.1. *The likelihood ratio $d(\mathbf{u})$ is the density of the random vector \mathbf{U} and*

$$E[\hat{\boldsymbol{\theta}}] = \boldsymbol{\theta} \quad \text{and} \quad \text{Cov}(\hat{\boldsymbol{\theta}}) = \boldsymbol{\Sigma} \quad (7)$$

where $\boldsymbol{\Sigma}$ has diagonal elements $\frac{\sigma_k^2}{n} = \frac{1}{n} V[T_k(\mathbf{U})]$ and non-diagonal elements $\frac{\sigma_{k,h}}{n} = \frac{1}{n} \text{Cov}[T_k(\mathbf{U}), T_h(\mathbf{U})]$, with $k, h \in \mathcal{K}$. Furthermore, if $F \equiv G$, the equalities in (7) reduce to

$$E[\hat{\boldsymbol{\theta}}] = \mathbf{0} \quad \text{and} \quad \text{Cov}(\hat{\boldsymbol{\theta}}) = \frac{1}{n} \mathbf{I}_M, \quad (8)$$

where $\mathbf{0}$ is the $M \times 1$ zero vector and \mathbf{I}_M is the $M \times M$ identity matrix.

Finally, an estimator of $d(\mathbf{u})$ is

$$\hat{d}(\mathbf{u}) = 1 + \hat{\boldsymbol{\theta}}' \mathbf{T}(\mathbf{u}), \quad (9)$$

and has variance $V[\hat{d}(\mathbf{u})] = \mathbf{T}(\mathbf{u})' \boldsymbol{\Sigma} \mathbf{T}(\mathbf{u})$.

It is worth pointing out that, when the likelihood ratio is formulated as a density, it is often referred to as *comparison density* (e.g., Parzen, 2004).

Combining (1), (2) and (9) an estimate of f is

$$\hat{f}(\mathbf{x}) = g(\mathbf{x}) \hat{d}(\mathbf{G}_R(\mathbf{x})) = g(\mathbf{x}) [1 + \hat{\boldsymbol{\theta}}' \mathbf{T}(\mathbf{G}_R(\mathbf{x}))] \quad (10)$$

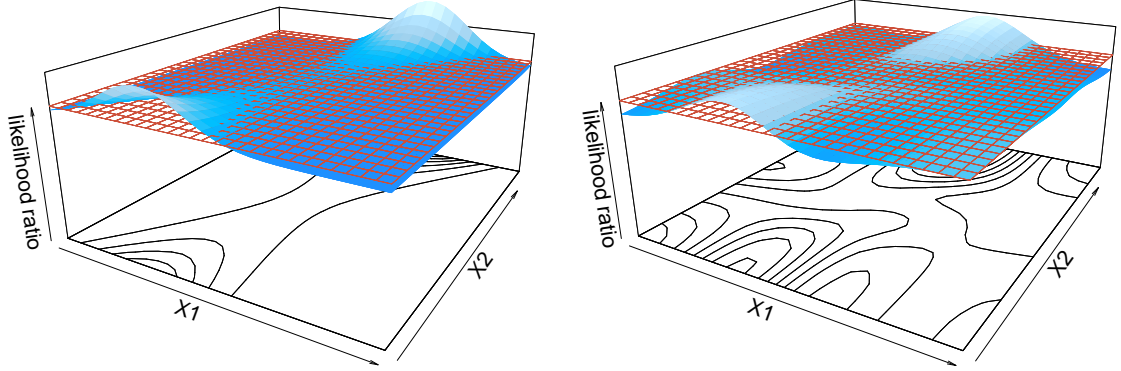


Figure 1: True (left panel) and estimated (right panel) likelihood ratio for Example I. The estimate on the right has been obtained via (9) with $m_1 = 4$ and $m_2 = 3$. The components of the $\hat{\theta}$ vector have been selected via the AIC criterion in (19).

Notice that the estimator \hat{f} incorporates the information carried by the hypothesized model g ; whereas, the estimator in the square brackets provides a data-driven correction for it. Furthermore, define the integrated squared bias (ISB) of $\hat{d}(\mathbf{u})$ to be

$$ISB = \int_{[0,1]^p} \left(E[\hat{d}(\mathbf{u})] - d(\mathbf{u}) \right)^2 d\mathbf{u}. \quad (11)$$

From Proposition 3.2 it follows that the closer g is to f in terms of squared normalized distance the lower the ISB of $\hat{d}(\mathbf{u})$.

Proposition 3.2. *The integrated squared bias of the estimator in (9) is*

$$\int_{[0,1]^p} \left(\frac{f(Q(\mathbf{u})) - g(Q(\mathbf{u}))}{g(Q(\mathbf{u}))} \right)^2 d\mathbf{u} - \theta' \mathbf{1}, \quad (12)$$

where $\mathbf{1}$ is the $M \times 1$ unit vector.

The estimate in (10) is essentially that of a smooth model (e.g., Rayner and Best, 1990), that is, a smoothed version of the true underlying probability function. Similarly to the smooth model proposed by Barton (1953) in the univariate setting, the estimator in (10) may lead to estimate that are not *bona-fide*, i.e, they may be negative and/or they

may not integrate/sum up to one. In this manuscript we focus on (10) mostly for the sake of mathematical convenience in deriving the inferential results of Section 4. Nonetheless, bona-fide estimators can be constructed similarly to the univariate case as described in Algeri and Zhang (2020).

Example I. In direct searches for dark matter, the dominant background sources are neutron recoils which may produce signals mimicking those expected from dark matter candidates (e.g., Westerdale, 2016). As a toy example, suppose we are interested in assessing the validity of a given distribution for the nuclear recoil background specified over the energy region $\mathcal{X} = [5, 20]KeVnr \times [0, 17]KeVnr$. Each observations in \mathcal{X} corresponds to the scintillation of photons (X_1) and ionization electrons (X_2) (e.g., Aprile et al., 2017). The hypothesized background distribution, $G_{X_1X_1}$, is that of a truncated bivariate normal with mean vector (12, 8), variances 8 and 12 and covariance 2. Moreover, suppose that one additional background source is present. The latter is also a bivariate normal with the same mean vector, variances 4 and 20 and covariance 5. Thus, the true model, $F_{X_1X_1}$, involves a mixture of two, overlapping truncated bivariate Gaussians with mixture parameter 0.15. In order to estimate the likelihood ratio, set $G_1 = G_{X_1}(x_1)$ and $G_2 = G_{X_2|X_1}$. The estimated likelihood ratio, obtained over a sample of $n = 5,000$, is shown in the right panel of Figure 1, whereas the left panel shows the true likelihood ratio. A closed form expression for the estimate shown on the right panel is given in equation ?? in the Supplementary Material.

While the estimate obtained recovers the main departures from uniformity, the contours highlight that the estimator is rather noisy. Therefore, it is important to investigate the properties of (9) to assess the significance of the deviations observed.

4 Inference and model selection

4.1 Pre-selection inference

A smooth test for $H_0 : G \equiv F$ versus $H_1 : G \not\equiv F$ consists in reformulating the problem as a test for uniformity of \mathbf{U} . Specifically, (2) implies that $F \equiv G$ whenever $d(\mathbf{u}) = 1$, and thus

$$H_0 : d(\mathbf{u}) = 1 \quad \forall \mathbf{u} \in [0, 1]^p \quad \text{versus} \quad H_1 : \exists \mathbf{u} \in [0, 1]^p \text{ s.t. } d(\mathbf{u}) \neq 1. \quad (13)$$

It is easy to see that $d(\mathbf{u}) = 1$ for all $\mathbf{u} \in [0, 1]^p$, when all θ_k , $k \in \mathcal{K}$, are identically equal to zero. Hence, in practice, we test

$$H_0 : \boldsymbol{\theta} = \mathbf{0} \quad \text{vs} \quad H_1 : \boldsymbol{\theta} \neq \mathbf{0}. \quad (14)$$

Notice that H_0 in (13) implies H_0 in (14), but the opposite is not true in general. Whereas, H_1 in (14) does imply H_1 in (13).

With a little abuse of nomenclature, in this section and those to follow, we will refer to G as the “null model”. Furthermore, we will refer to H_0 in (13) when generically saying “under H_0 ”. However, most of the results presented here, only require validity of the milder H_0 in (14).

To conduct our inference, we consider the so-called *deviance* test statistics, i.e.,

$$D = n\widehat{\boldsymbol{\theta}}'\widehat{\boldsymbol{\theta}}. \quad (15)$$

Its asymptotic null distribution is given in Theorem 4.1.

Theorem 4.1. *If H_0 is true, then*

$$\sqrt{n}\widehat{\boldsymbol{\theta}} \xrightarrow{d} N(\mathbf{0}, \mathbf{I}), \quad \text{as } n \rightarrow \infty \quad (16)$$

where $N(\mathbf{0}, \mathbf{I})$ denotes a standard multivariate normal distribution. Furthermore,

$$D \xrightarrow{d} \chi_M^2, \quad \text{as } n \rightarrow \infty, \quad (17)$$

where M is the length of $\widehat{\boldsymbol{\theta}}$.

Corollary 4.2 follows directly from Theorem 4.1.

Corollary 4.2. Denote with $\{\widehat{d}(\mathbf{u})\}$ the random field indexed by $\mathbf{u} \in [0, 1]^p$ with components as in (9). Moreover, assume that $\widehat{\theta}_k = o(n^{-1/2})$ for all $k \notin \mathcal{K}$. If H_0 is true,

$$\left\{ \frac{\widehat{d}(\mathbf{u}) - 1}{\sqrt{\frac{1}{n} \mathbf{T}(\mathbf{u})' \mathbf{T}(\mathbf{u})}} \right\} \xrightarrow{d} \mathbf{Z}(\mathbf{u}), \quad \text{as } n \rightarrow \infty, \quad (18)$$

where $\mathbf{Z}(\mathbf{u})$ denotes a Gaussian random field with mean zero, unit variance and covariance function $\text{Cov}(\mathbf{Z}(\mathbf{u}), \mathbf{Z}(\mathbf{u}^\dagger)) = \frac{\mathbf{T}(\mathbf{u})' \mathbf{T}(\mathbf{u}^\dagger)}{\sqrt{\mathbf{T}(\mathbf{u})' \mathbf{T}(\mathbf{u}) \mathbf{T}(\mathbf{u}^\dagger)' \mathbf{T}(\mathbf{u}^\dagger)}}$.

At this stage, constructing inference on the basis of Theorem 4.1 and Corollary 4.2 would be tempting. However, to guarantee the validity of our results we must take into account that, when estimating the likelihood ratio in (9), a model selection procedure is likely to be implemented. Unfortunately, when a model is selected by a pool of possibilities, such process introduces an additional source of variability and thus the resulting inference is automatically affected (e.g., Berk et al., 2013). Section 4.2 addresses this aspect directly.

4.2 Post-selection inference

The estimate of the likelihood ratio considered so far involves up to M functions $T_k(\mathbf{u})$. Nonetheless, it is possible that not all of these M terms are needed to capture the departures of G from F and indeed, it is often convenient to remove some of them in order to avoid unnecessary sources of noise. Various criteria have been proposed in literature for density estimation and smooth models (e.g., Mukhopadhyay, 2017; Algeri,

2020) and which can be easily extended to the multivariate setting. Here, we focus on the approach of Mukhopadhyay (2017) and which specifies as follows.

Let $\widehat{\theta}_{(k)}$ be the k^{th} largest $\widehat{\theta}_k$ estimate in order of magnitude, i.e., $\widehat{\theta}_{(1)}^2 \geq \widehat{\theta}_{(2)}^2 \geq \dots \geq \widehat{\theta}_{(M)}^2$. Select the K largest coefficients which maximize either

$$\text{BIC}(K) = \sum_{(k)=1}^K \widehat{\theta}_{(k)}^2 - \frac{K \log n}{n} \quad \text{or} \quad \text{AIC}(K) = \sum_{(k)=1}^K \widehat{\theta}_{(k)}^2 - \frac{2K}{n}. \quad (19)$$

Notice that, as defined in (5), each k is a p -tuple of indexes $j_1 \dots j_p$, whereas (k) is the integer value corresponding to the order of magnitude of the respective coefficient $\widehat{\theta}_k$. Hence, the summations in (19) and those to follow are taken over $(k) = 1, \dots, K$, that is the K p -tuples of indexes $j_1 \dots j_p$ with the K^{th} largest estimates $\widehat{\theta}_k$.

An estimate of $d(\mathbf{u})$, is then selected via (19) from the family of estimators

$$\widehat{d}_{(K)}(\mathbf{u}) = 1 + \sum_{(k)=1}^K \widehat{\theta}_{(k)}^2 T_{(k)}(\mathbf{u}), \quad K=1, \dots, M \quad (20)$$

where the subscript (K) is used to emphasize that the estimator in (20) includes only the K^{th} largest $\widehat{\theta}_k$ estimated coefficients. Clearly, the choice of BIC or AIC is arbitrary and, from a practical standpoint, the BIC tends to lead to smoother estimates than the AIC.

The selection rules in (19) compare M possible models assuming that each m_d , for $d = 1, \dots, D$ was fixed before the researcher looked at the data. Valid post-selection inference can then be constructed as in Theorem 4.1 and Corollary 4.3. The respective proofs are provided in the Supplementary material.

Corollary 4.3. Denote with $\widehat{d}_{(K^*)}$ the estimator of $d(\mathbf{u})$ selected via (19), and let $D_{(K^*)} = \sum_{(k)=1}^{K^*} \widehat{\theta}_{(k)}^2$ be the respective deviance statistics. As $n \rightarrow \infty$, a valid post-

selection bound for the p -value to test (13) is

$$p\text{-value}_{adj} = P(\chi_M^2 > D_{obs}), \quad (21)$$

where D_{obs} is the value of $D_{(K^*)}$ observed.

Where the bound in (21), follows from the fact that the estimators in (20) are nested, for all $K = 1, \dots, M-1$, and thus each $D_{(K)}$ is stochastically lower or equal than $D_{(M)}$. Hence, for all $K = 1, \dots, M-1$, $P(D_{(K)} > D_{obs})$ is smaller than $P(D_{(M)} > D_{obs})$.

In order to grasp further insights on the deviations of G from F , it is worth constructing adequate confidence bands. This can be done, while accounting for post-selection adjustments, as in Corollary 4.4.

Corollary 4.4. Denote with $\widehat{d}_{(K^*)}$ the estimator of $d(\mathbf{u})$ selected via (19), and denote with $SE_0[\widehat{d}_{(K^*)}(\mathbf{u})]$ its standard error under H_0 . Valid (post-selection adjusted) $(1-\alpha)\%$ confidence regions, under H_0 in (13), are

$$\left[1 - c_{\alpha/2} SE_0[\widehat{d}_{(K^*)}(\mathbf{u})], 1 + c_{\alpha/2} SE_0[\widehat{d}_{(K^*)}(\mathbf{u})] \right] \quad \text{for all } \mathbf{u} \in [0, 1]^p \quad (22)$$

with $c_{\alpha/2}$ such that

$$P\left(\sup_{\mathbf{u}} \left\{ \frac{\widehat{d}_{(M)}(\mathbf{u}) - 1}{SE_0[\widehat{d}_{(M)}(\mathbf{u})]} \right\} > c_{\alpha/2} \middle| H_0\right) = \frac{\alpha}{2}. \quad (23)$$

Intuitively, $\widehat{d}_{(M)}$ is the least smooth among all the estimators considered; hence, we expect that the random field resulting from $\widehat{d}_{(M)}$ has the largest probability of crossing the fixed level $c_{\alpha/2}$.

From a theoretical perspective, a highly non-trivial aspect in the construction of (22) is the estimation of the quantile $c_{\alpha/2}$. Probabilities such (23) are known in literature as *excursion probabilities* (e.g., Adler, 2000) and which cannot be expressed in closed form.

A possible solution for constructing the confidence bands in (22), is that of proceeding by estimating $SE_0[\widehat{d}_{(K^*)}(\mathbf{u})]$ and $c_{\alpha/2}$ via Monte Carlo simulations (see Algeri and Zhang, 2020, Algorithm 1). Unfortunately, in the most crucial (astro)physical searches the level of significance required to claim a new discovery is typically in the order of $\alpha = 10^{-7}$ (e.g., Lyons, 2013), and thus Monte Carlo simulations may be computationally prohibitive. This is further aggravated when dealing with complex models for which even a single Monte Carlo replicate can be highly expensive in terms of both computational and time resources.

As a valid alternative, for continuous F and G , accurate approximations for (23) under mild smoothness conditions exist (e.g., Taylor and Worsley, 2008). In our setting, smoothness follows from the fact that the random field in (18) and the respective limit can be written as a linear combination of the functions $\frac{T_k(\mathbf{u})}{\sqrt{\sum_{k \in \mathcal{K}} T_k^2(\mathbf{u})}}$ (see proof of Corollary 4.2 in the Supplementary Material) which are composition of Legendre polynomials, and thus, admit infinite partial derivatives.

An approximation for the left-hand side of (23) is

$$(1 - \Phi(c_{\alpha/2})) + \mathcal{L}_1 \frac{e^{-\frac{c_{\alpha/2}^2}{2}}}{\pi} + \mathcal{L}_2 \frac{e^{-\frac{c_{\alpha/2}^2}{2}}}{\sqrt{2\pi^{3/2}}} + O\left(\exp\left(-\frac{\gamma c_{\alpha/2}^2}{2}\right)\right), \quad \text{as } n \rightarrow \infty, \quad (24)$$

for some $\gamma > 1$ (Taylor et al., 2005). In (24), \mathcal{L}_1 and \mathcal{L}_2 are constant known as Lipschitz-Killing curvatures and are typically estimated numerically (e.g., Algeri and van Dyk, 2020). Notice that the error rate in (24) decreases exponentially fast, as $\alpha \rightarrow \infty$. Therefore, this solution is particularly amenable to overcome the issues arising when dealing with stringent significance requirements.

As one may expect, the simplicity of the post-selection adjustments in (21) and (22) comes with a price. Specifically, they can be rather conservative for increasing values of M . However, as shown below for Example I and in the sections to follow, (21) still leads to high power even if the sample size is only moderately large. Similarly, (22) can be

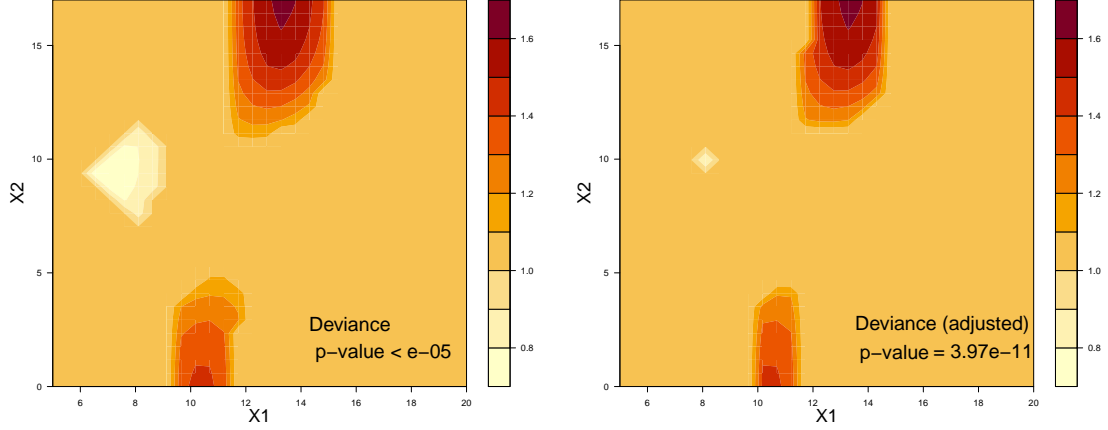


Figure 2: Simulated and approximated confidence regions for Example I. The left panel corresponds to the (post-selection) confidence regions and deviance p -value obtained via a simulation of size $B = 10,000$. The right panel shows to the (post-selection adjusted) confidence regions and deviance p -value computed as in (21) and (22). Darker shades correspond to significant deviations of the estimated likelihood ratio above one. Lighter shades correspond to significant deviations below one.

	$n = 500$	$n = 1000$	$n = 2000$	$n = 5000$	$n = 7000$	$n = 10,000$
Type I error (\pm SE)	0.0540 (± 0.0023)	0.0500 (± 0.0022)	0.0499 (± 0.0022)	0.0482 (± 0.0021)	0.0508 (± 0.0022)	0.04930 (± 0.0022)
Power (\pm SE)	0.2157 (± 0.0041)	0.4456 (± 0.0050)	0.8063 (± 0.0040)	0.9995 (± 0.0002)	1.0000 (± 0.0000)	1.0000 (± 0.0000)

Table 1: Simulated probability of type I error and power for Example I considering different sample sizes. The nominal level is chosen to be $\alpha = 0.05$. Each simulation involves $B = 10,000$ replicates.

quite accurate and match closely the confidence regions obtained by simulating directly the distribution of (18), while repeating the selection process at each replicate.

Example I (continued). The estimate of the likelihood ratio in the right panel of Figure 1 has been obtained by setting $m_1 = 4$ and $m_2 = 3$ and selecting the terms of the respective tensor basis via the AIC rule in (19). The AIC procedure selects 9 terms out of $M = 19$. The post-selection adjusted p -value and 95% confidence regions are shown in the right panel of Figure 2. The confidence contours are constructed by setting equal to one all the values of \hat{d} contained within the bands in (22). Whereas the quantile c_α

has been calculated by solving

$$(1 - \Phi(c_{\alpha/2})) + \mathcal{L}_1 \frac{e^{-\frac{c_{\alpha/2}^2}{2}}}{\pi} + \mathcal{L}_2 \frac{e^{-\frac{c_{\alpha/2}^2}{2}}}{\sqrt{2}\pi^{3/2}} - \frac{\alpha}{2} = 0 \quad (25)$$

and estimating \mathcal{L}_1 and \mathcal{L}_2 by means of the R package TOHM (Algeri, 2019) as described in Algeri and van Dyk (2020). This approach led to $c_{\alpha} = 3.5568$. The confidence contours suggest that the most prominent deviations occur in correspondence of the regions $[10, 12] \times [0, 5]$ and $[12, 15] \times [12, 17]$. Here, the estimator of $d(\mathbf{u})$ shows significant deviations above one and thus we conclude that the postulated model underestimates the truth over these areas. The presence of significant departures of $G_{X_1 X_2}$ from $F_{X_1 X_2}$ are confirmed by the deviance test (adjusted p-value $\sim 3.97 \cdot 10^{-11}$). The left panel of Figure 2 shows the confidence regions and deviance p-value obtained by means of a Monte Carlo simulation involving $B = 10,000$ replicates. The selection procedure has been implemented at each replicate. While more conservative, the confidence regions computed via (22) and (25), approximate reasonably well those obtained via simulation.

Finally, we investigate the probability of type I error and the power of the deviance test based on (21). Table 5 reports the results obtained considering a suite of five simulations, each of size $B = 10,000$, conducted using five different sample sizes. For all n considered, the probability of type I error observed is approximately the same than the nominal level $\alpha = 0.05$. Whereas, the power increases rapidly with n . For the smallest samples sizes considered, i.e., $n = 500$ and $n = 1000$, the power is rather low ($\sim 22\%$ and $\sim 45\%$, respectively). However, it has to be noted that, in our example, the mixture parameter is 0.15; therefore the deviations from the postulated model effectively account for only ~ 75 and ~ 150 data points when $n = 500$ and $n = 1000$, respectively.

In principle the plots in Figures 1, 2, and those to follow, could also be visualized in the quantile domain. The latter is to be preferred when working with long tailed distribution where one may expect that only a few observations have been detected over

large regions of the \mathbf{X} domain. In those situations, the quantile representation would allow to magnify the differences observed over the the most “data-abundant” regions. An more detailed discussion of this aspect, and adequate graphical comparisons can be found in (Algeri, 2020).

5 iGOF-diagnostic analysis

The constructs introduced so far allow us to assess the validity of the postulated model, obtain an estimate of the likelihood ratio test to visualize where and how departures of g from f occur, and construct a data driven correction for the initial model g (equation 10). Unfortunately, however, a visual inspection is only possible when $p \leq 3$. Nevertheless, when $p > 3$, more insights on the sources of mismodeling affecting G can be obtained by conducting an ANOVA-like analysis where random sub-vectors of \mathbf{X} are tested individually, from the largest to the smallest.

Without loss of generality, let $\mathbf{X}_q = (X_1, \dots, X_q)$ be the random collecting the first $q < p$ components of \mathbf{X} . Denote with F_q the true cdf of \mathbf{X}_q and let G_q be its postulated cdf. Moreover, assume that the density of G_q can be specified as

$$g_q(\mathbf{x}_q) = \prod_{d=1}^q g_d(x_d | \mathbf{x}_{<d}) \quad \text{for all } d = 1, \dots, q. \quad (26)$$

Similarly to (2) and (4), we can then express the likelihood ratio of \mathbf{X}_q on the q dimensional unit cube via

$$d(\mathbf{u}_q) = \frac{f_q(\mathbf{Q}_q(\mathbf{u}_q))}{g_q(\mathbf{Q}_q(\mathbf{u}_q))} = \sum_{j_1 \geq 0, \dots, j_q \geq 0} \theta_{j_1 \dots j_q} T_{j_1 \dots j_q}(\mathbf{u}_q), \quad \mathbf{u}_q \in [0, 1]^q \quad (27)$$

where $\mathbf{u}_q = (G_1(x_1), \dots, G_q(x_q | \mathbf{x}_{<q}))$, and thus \mathbf{u}_q is a sub-vector of $\mathbf{u} = \mathbf{G}_R(\mathbf{x})$.

Whereas, similarly to (3), one can write the tensor basis functions $T_{j_1 \dots j_q}$ as

$$T_{j_1 \dots j_q}(\mathbf{u}_q) = \prod_{d=1}^q T_{j_d}(u_d) = \prod_{d=1}^p T_{j_d}(u_d) \quad \text{with } j_d = 0, \text{ for all } d = q+1. \quad (28)$$

The last equality follows from the fact that $T_0(G(x_d|\mathbf{x}_{<d})) = 1$ for all $d = 1, \dots, p$, and thus each $T_{j_1 \dots j_q}(\mathbf{u}_q) = T_{j_1 \dots j_q 0 \dots 0}(\mathbf{u})$. Consequently, the $\theta_{j_1 \dots j_q}$ coefficients are equal to the theta $\theta_{j_1 \dots j_p}$ whenever $j_d = 0$, for all $d = q+1$. As a result, we can easily perform inference for \mathbf{X}_q by means of the estimators $\hat{\theta}_k$ in (6), without the need of an entirely new estimation procedure.

Specifically, denote with \mathcal{K}_q and \mathcal{K}^* the subsets of \mathcal{K} in (5)

$$\mathcal{K}_q := \left\{ k = \{j_1 \dots j_p\} \in \mathcal{K} \text{ with } j_d = 0, \text{ for all } d = q+1, \dots, p \right\} \quad (29)$$

$$\mathcal{K}^* := \left\{ k = \{j_1 \dots j_p\} \in \mathcal{K} \text{ with } (k) \leq K^* \right\} \quad (30)$$

of cardinality $|\mathcal{K}_q| = M_q = \prod_{d=1}^q (m_d + 1) - 1$ and $|\mathcal{K}^*| = K^*$. Recall that K^* is the value minimizing either the AIC or BIC in (19), and thus, \mathcal{K}^* collects all the p -tuple of indexes in \mathcal{K} which have been ultimately selected when constructing the estimator $\hat{d}_{(K^*)}$ and the deviance statistics $D_{(K^*)}$ in Corollaries 4.3 and 4.4. To test

$$H_0 : G_q = F_q \quad \text{versus} \quad H_1 : G_q \neq F_q \quad (31)$$

we may consider the test statistics $D_q = n \sum_{k \in \mathcal{K}_q} \hat{\theta}_k^2$ and proceed as in Theorem 4.1. Whereas, valid post-selection inference can be obtained as in Theorem 5.1.

Theorem 5.1. *As $n \rightarrow \infty$, a valid post-selection bound for the p -value to test (31) is*

$$p\text{-value}_{q,adj} = P(\chi_{M_q}^2 > D_{obs}), \quad (32)$$

where D_{obs} being the value of the test statistics

$$D_q^* = n \sum_{k \in \mathcal{K}_q \cap \mathcal{K}^*} \hat{\theta}_k^2 \quad (33)$$

observed, \mathcal{K}_q and \mathcal{K}^* as in (29) and (30) and $\hat{\theta}_k$ as in (6).

Theorem 5.1 follows directly from (27) and (28) and, in virtue of the orthogonality of the T_k functions and condition (26).

Remark 5.2. Because of condition (26), Theorem 5.1 holds only for random sub-vectors of \mathbf{X} whose Rosenblatt transform u_q includes all the conditioning, from the higher to the lower, necessary to recover $g_q(\mathbf{x}_q)$. To some extent, this condition can be seen as the iGOF counterpart of the marginality principle advocated by Nelder (1977) in the context of ANOVA, and which consists in taking into account of the hierarchy of the main effects and interactions in a given model.

Similarly to the ANOVA, Theorem 5.1 allows us to construct an iGOF-diagnostic table to identify the source of misspecification for a given random vector \mathbf{X} and its components. Below we show how this can be done in practice for the case of a 7-dimensional random vector.

Example II. We consider a sample of $n = 5000$ observations from a random vector $\mathbf{X} = (X_1, \dots, X_7)$ with components distributed as summarized in the second column of Table 2. Table 3 collects the results obtained by applying Theorem 5.1 to test the validity of the models specified for different sub-vectors of \mathbf{X} . The overall deviance test is reported in the first row and correctly reject the null model.

Similarly, the test in the second row, rejects the hypotheses that the vector (X_1, X_2, X_5, X_6) is modelled correctly, and fails to reject the model for (X_1, X_2, X_5) . This aspect is particularly important as it highlights that the misspecification occurs only with respect to the

Variable	True (F)	Hypothesized (G)	Correct
$X_6 X_1, X_2, X_5$	$\text{Laplace}\left[e^{0.03x_1+0.02x_2+0.01x_2^2+0.02x_5}, 1\right]$	$\text{Laplace}\left[e^{0.03x_1+0.02x_2+0.02x_5}, 1\right]$	No
X_1, X_2, X_5	$N\left[\begin{pmatrix} 10 \\ 15 \\ 11 \end{pmatrix}, \begin{pmatrix} 4 & 0.5 & 0 \\ 0.5 & 3 & 1 \\ 0 & 1 & 5 \end{pmatrix}\right]$	$N\left[\begin{pmatrix} 10 \\ 15 \\ 11 \end{pmatrix}, \begin{pmatrix} 4 & 0.5 & 0 \\ 0.5 & 3 & 1 \\ 0 & 1 & 5 \end{pmatrix}\right]$	Yes
$X_4 X_3$	$\text{Exponential}\left(\frac{1}{x_3}\right)$	$\text{Exponential}\left(\frac{1}{x_3}\right)$	Yes
X_3	$\text{Exponential}(1)$	$\text{Exponential}(0.9)$	No
X_7	T_3	$\text{Cauchy}(0, 1)$	No

Table 2: True and postulated model for Example II. The last column highlights where mismodeling occurs.

conditional distribution of $X_6|X_1, X_2, X_5$. The tests in the fourth and fifth row show that the vector (X_3, X_4) has been mismodeled and one source of mismodeling is the marginal of X_3 . Ultimately, the test for X_7 also correctly rejects the null hypothesis of Cauchy distribution. Table 4 collects the results of a simulation obtained by repeating the diagnostic analysis in Table 3 through a simulation of $B = 10,000$ replicates, while considering different sample sizes. Even when the sample size considered is only 500, the most prominent deviations are captured with probability one, whereas, the model for (X_1, X_2, X_5) is never rejected. More issues arise in diagnosing mismodeling of X_3 and, consequently, (X_3, X_4) for smaller samples. For instance, even when $n = 1000$ the power of the procedure in detecting departures of G_{X_3} from F_{X_3} is only $\sim 56\%$ and $\sim 3\%$ for (X_3, X_4) . It has to be noted, however, that detecting mismodeling of X_3 is a particularly challenging task. As shown in Figure 3, the postulated and the true pdf of X_3 are very close one-another; this minor differences are further “diluted” when considering the joint distribution of (X_3, X_4) , since $X_4|X_3$ is correctly specified. Nevertheless, such minor deviations are detected with high power for larger sample sizes.

\mathbf{X}_q	df	(Adjusted) p-value
\mathbf{X}	16383	$< 10^{-130}$
(X_1, X_2, X_5, X_6)	256	$< 10^{-130}$
(X_1, X_2, X_5)	63	1
(X_3, X_4)	15	$8.467 \cdot 10^{-08}$
X_3	3	$1.525 \cdot 10^{-13}$
X_7	3	$2.599 \cdot 10^{-122}$

Table 3: *i*GOF-diagnostic table. The third column reports the (post-selection adjusted) deviance p-values in (32) with \mathbf{X}_q specified as in the first column. The second column corresponds to the degrees of freedom used in the calculation of the p-value, namely, M_q .

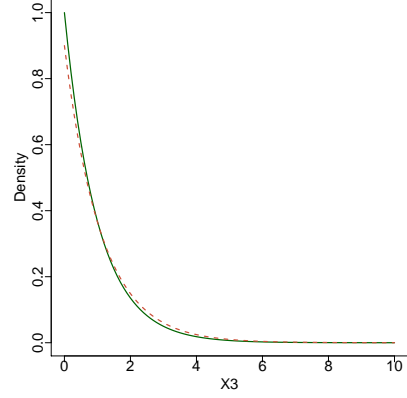


Figure 3: Comparing the postulated (red dashed line) and the true model (green solid line) of X_3 .

\mathbf{X}_q	Sample size (n)					
	500	1000	2000	3000	5000	10,000
\mathbf{X}	1	1	1	1	1	1
(X_1, X_2, X_5, X_6)	1	1	1	1	1	1
(X_1, X_2, X_5)	0	0	0	0	0	0
(X_3, X_4)	0.0069 (± 0.0008)	0.0342 (± 0.0018)	0.2384 (± 0.0049)	0.5939 (± 0.0049)	0.9615 (± 0.0019)	1
X_3	0.2360 (± 0.0043)	0.5560 (± 0.0050)	0.9153 (± 0.0028)	0.9868 (± 0.0011)	0.9999 (± 0.0001)	1
X_7	1	1	1	1	1	1

Table 4: Performance of the *i*GOF-diagnostic analysis for different sample sizes. For values different from zero and one the Monte Carlo errors ($\pm SE$) are also reported. The significance level considered is $\alpha = 0.05$.

6 A diagnosis of background mismodeling

When conducting searches for new phenomena, mismodeling of the background distribution can dramatically compromise the sensitivity of the experiment. Specifically, overestimating the background can increase the chances of false negatives. Whereas, underestimating the background may lead to claiming false discoveries. To illustrate how *i*GOF can be used to understand if and how the postulated background model have been mis-specified, we consider a simulated observation by the Fermi Large Area Telescope (LAT)

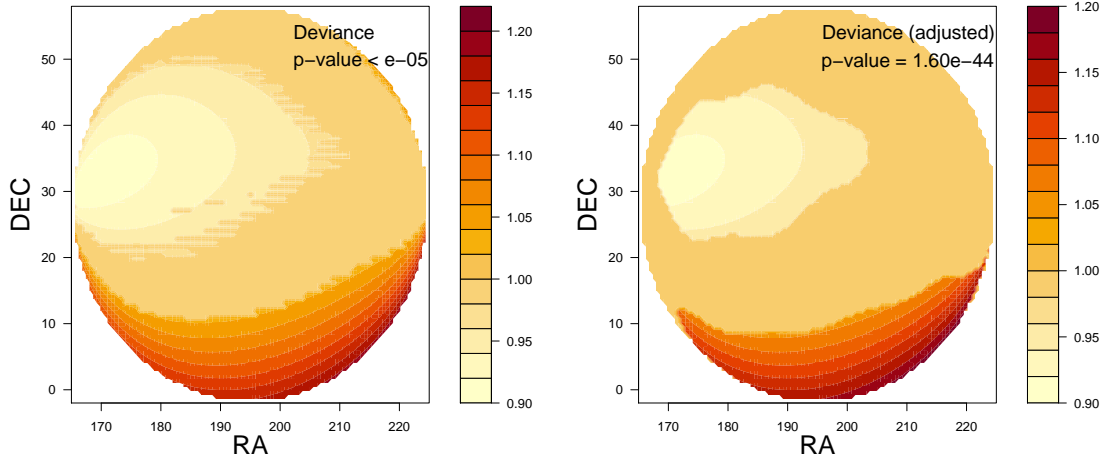


Figure 4: Simulated and approximated confidence regions for the Fermi LAT simulation. The left panel corresponds to the (post-selection) confidence regions and deviance p -value obtained via a simulation of size $B = 10,000$. The right panel shows to the (post-selection adjusted) confidence regions and deviance p -value computed as in (21) and (22). Darker shades correspond to significant deviations of the estimated likelihood ratio above one. Lighter shades correspond to significant deviations below one.

Atwood et al. (2009) obtained with the *gtobssim* package² and previously published in Algeri and van Dyk (2020). The simulation includes a realistic representations of the instrumental noise of the detector and present backgrounds.

The region of interest corresponds to a disc in the sky of 30° radius and centered at (195 RA, 28 DEC), where RA and DEC are the coordinates in the sky. Here we assume that, despite the cosmic background is known to follow a uniform distribution over the search area, it is unclear if the instrumental error is effectively negligible, or if it has a prominent effect on the underlying distribution. Therefore, we set $G_{X_1 X_2}$ to be the cdf of a uniform distribution with support $\mathcal{X}_1 \times \mathcal{X}_2 = [165, 195] \times [28 - \sqrt{30^2 - (x - 195)^2}, 28 + \sqrt{30^2 - (x - 195)^2}]$ and we proceed by estimating the likelihood ratio via (9) over a sample of $n = 68658$ observations. Specifically, we set $m_1 = m_2 = 4$ and we select the

²<http://fermi.gsfc.nasa.gov/ssc/data/analysis/software>

components of $\hat{\theta}$ via the BIC criterion in (19). The resulting estimate is

$$\hat{d}(G_1(x_1), G_2(x_2|x_1)) = 1 + 0.022T_1(G_1(x_1)) - 0.043T_1(G_2(x_2|x_1)) + 0.041T_2(G_2(x_2|x_1)). \quad (34)$$

In order to assess the significance of the deviations captured by (34), we compute both the confidence regions and deviance p-values via (22) and (21). The results are reported in the right panel of Figure 4, whereas the left panel shows the confidence regions and deviance p-value obtained via simulation. Similarly to what we have observed for Example I (see Figure 2), despite the approximate confidence bands are more conservative, they still allow to capture the main departures from uniformity. Indeed, in both cases, we can see that the prominent deviations of the true underlying model from the postulated uniform distribution occur in proximity of low values of X_2 . Whereas, at the center-left of the search area, the uniform model significantly underestimates the model inclusive of the instrumental error. Finally, it follows from (10) that an updated model background distribution which accounts for these deviations can be constructed as in (10) by simply multiplying the uniform pdf by the estimated likelihood ratio in (34).

7 Extensions to the discrete case

The methods discussed so far focus on the case where F and G are continuous. However, extensions to the discrete setting can be derived by rewriting the expansion in (4) through an orthonormal set of functions suitable to model discrete data. This can be done, for instance, by means of the so-called “LP³ score functions”, recently introduced (e.g., Mukhopadhyay and Wang, 2020) and which can be seen as a generalization of the Legendre polynomials valid in both the continuous and discrete setting.

Specifically, when $p = 1$, a complete orthonormal basis of LP score functions in

³In the *LP* acronym, the letter *L* typically denotes nonparametric methods based on quantiles, whereas *P* stands for polynomials (Mukhopadhyay and Wang, 2020, Supp S1).

$L^2(G)$ can be specified by letting the first component to be $T_0[G(x)] = 1$. Subsequent components $\{T_j[G(x)]\}_{j>0}$ are obtained by Gram-Schmidt orthonormalization of powers of

$$T_1[G(x)] = \frac{G_{\text{mid}}(x) - E[G_{\text{mid}}(x)]}{\sqrt{V(G_{\text{mid}}(x))}} = \frac{G(x) - 0.5p_G(x) - 0.5}{\sqrt{[1 - \sum_{x \in \mathcal{X}} p_G^3(x)]/12}}, \quad (35)$$

where $G_{\text{mid}}(x) = G(x) - 0.5p_G(x)$ is the *mid-distribution function*, which it has been shown in Parzen (2004) to have mean 0.5 and variance $[1 - \sum_{x \in \mathcal{X}} p_G^3(x)]/12$, with \mathcal{X} being the set of distinct points in the support of X and $p_G(x) = P(X = x)$ if $X \sim G$. Therefore, $T_1[G(x)]$ is the standardized mid-distribution and orthonormality of the $T_j[G(x)]$ functions in $L^2(G)$ follows by the first equality in (35) and by Gram-Schmidt process.

Notice that, for continuous X , $G_{\text{mid}}(x) = G(x)$ and $\sum_{x \in \mathcal{X}} p_G^3(x) = 0$, consequently, the LP score functions reduce to normalized shifted Legendre polynomials. The latter are effectively the result of a Gram-Schmidt orthonormalization applied to powers of $G(x)$. Whereas, the LP score functions are obtained by orthonormalizing powers of the standardized mid-distribution function with respect to the measure G .

Recall that, in our context, the cdfs G_d , $d = 1, \dots, p$ are the conditional and marginal distribution functions specified in the Rosenblatt's transform $\mathbf{G}_R(\mathbf{x})$. Hence, an orthonormal basis in $L^2(G_d)$ is $\{T_{j_d}[G_d(\cdot|\cdot)]\}_{j_d \geq 0}$ with $T_0[G_d(x_d|\mathbf{x}_{<d})] = 1$ and subsequent components

$$T_{j_d}[G_d(x_d|\mathbf{x}_{<d})] = \frac{\mathring{T}_{j_d}[G_d(x_d|\mathbf{x}_{<d})]}{\|\mathring{T}_{j_d}[G_d(x_d|\mathbf{x}_{<d})]\|_{G_d}}, \quad \text{for all } j_p \geq 1, \text{ where} \quad (36)$$

$$\mathring{T}_{j_d}[G_d(x_d|\mathbf{x}_{<d})] = T_1^{j_d}[G_d(x_d|\mathbf{x}_{<d})] \quad (37)$$

$$- \sum_{k=1}^{j_p-1} \langle T_1^{j_d}[G_d(x_d|\mathbf{x}_{<d})], T_k[G_d(x_d|\mathbf{x}_{<d})] \rangle_{G_d} T_k[G_d(x_d|\mathbf{x}_{<d})], \quad (38)$$

$$\langle T_1^{j_d}[G_d(x_d|\mathbf{x}_{<d})], T_{k_d}[G_d(x_d|\mathbf{x}_{<d})] \rangle_{G_d} = \quad (39)$$

$$\int T_1^{j_d}[G_d(x_d|\mathbf{x}_{<d})] T_{k_d}[G_d(x_d|\mathbf{x}_{<d})] dG_d(x_d|\mathbf{x}_{<d}) \quad (40)$$

and $\|\cdot\|_{G_d} = \sqrt{\langle \cdot, \cdot \rangle_{G_d}}$.

When $p > 1$ a suitable tensor basis in $L^2(G)$ can then be constructed as in Proposition 3. $\{T_{j_1, \dots, j_p}(\mathbf{u})\}_{j_1 \dots j_p \geq 0}$. Orthonormality of the $T_{j_1, \dots, j_p}(\mathbf{u})$ score functions can be verified directly as shown in Section ?? of the Supplementary Material.

8 Discussion

This work proposes an informative approach to goodness-of-fit which connects exploratory and confirmatory data analysis to study multivariate distributions. By transforming the likelihood ratio on the unit cube, confidence regions can be constructed as in Corollary 4.4 to identify regions of the support where significant deviations occurs. While this approach is practical only for problems in at most three dimensions, in more dimensions a detailed diagnosis of misspecification can be achieved by means of the iGOF-diagnostic analysis proposed in Section 5. These tools can be used to directly address Q1 in Section 1. For instance, given the panacea of theories available on the nature of dark matter, experimentalists aiming to detect it often face the dilemma of selecting which of the tens of theoretical models (mainly non-nested) available should be tested (e.g., [Scott, 2018](#)). If one was to test it using the procedure discussed in this paper, even when a given model

is rejected, it is possible to gain further insight on the shape of the departure of the true data distribution and the null model and ultimately use such information to “rule out” other models which would be inconsistent with such deviation.

Moreover, as we aimed for when formulating Q2 in Section 1, the true probability function of the data can be estimated semi-parametrically via (10), while assessing the validity of the model postulated by the scientists. Interestingly, the resulting estimate incorporates the knowledge carried by the hypothesized model and thus, it provides a data-driven update for it in the direction of the true distribution of the data.

Despite the usefulness of the methods presented here in applied settings, and in the physical sciences in particular (e.g., Section 6), they are not exempt from limitations. For instance, several problems in physics and astronomy, often involve no more than 8 or 10 dimensions and/or can be reduced to 2D planes (e.g., Aprile et al., 2017). In this context, choosing m_d equal to 3 or 4 for all $d = 1, \dots, p$, is often sufficient to avoid overfitting and, eventually, lack of power by implementing adequate model selection strategies and for sufficiently large samples (see Sections 4 and 5). In more dimensions, however, the method suffers from the curse of dimensionality (e.g. Friedman et al., 2001), as the size of the LP tensor basis increases exponentially fast with p . In this context, a regularized solution could be particularly valuable (see for instance Signoretto et al., 2014) when analyzing, for instance, data coming from large astronomical surveys such as the Large Synoptic Survey Telescope (LSST) survey (e.g., Tyson, 2002).

Furthermore, the unitary representation of the likelihood ratio in (2) relies on the Rosenblatt transform and which can lead to different configurations of \mathbf{U} and, potentially, different estimators. Despite this aspect would require adequate treatment on its own, it is worth noting that this problem is essentially the same arising in the context of vine copulas (e.g., Nagler et al., 2017) and for which adequate model selection procedures exists (e.g., Panagiotelis et al., 2017; Dissmann et al., 2013).

Finally, the inferential procedures presented here extend classical smooth tests to the

multivariate setting and allow us to visualize graphically the departure of F from G and study their substructures. Despite this article focuses on simple null hypothesis, that is, the postulated model is assumed to be fully specified, classical results on smooth tests (e.g., [Thas, 2010](#), Sec 4.2.2.3 and 5.2.2.3) can be used to show to derive asymptotic tests in the parametric setting. Unfortunately, however, the asymptotic approximations are known to be rather slow in the parametric case. Therefore, in practical applications, when G depends on unknown parameters it is recommended to perform inference by means of the parametric bootstrap and which has been shown by [Babu and Rao \(2004\)](#) to be consistent also in the multivariate setting.

Appendix

Symbol	Description
$\mathbf{X} = (X_1, \dots, X_p)$	Random vector of components $X_d, d = 1, \dots, p$
\mathcal{X}	Support of \mathbf{X}
F, f	True cdf and density of \mathbf{X}
G, g	Postulated cdf and density of \mathbf{X}
G_d, Q_d, g_d	Conditional cdf, quantile function and density of X_d
$\mathbf{U} = \mathbf{G}_R(\mathbf{X})$	Rosenblatt's transform of \mathbf{X}
$\mathbf{Q}(\mathbf{X}) = \mathbf{U}$	Inverse of the Rosenblatt's transform
$\mathbf{x} = (x_1, \dots, x_p) = \mathbf{Q}(\mathbf{u})$	Realization of \mathbf{X} with components $x_d = Q_d(u_d)$
$\mathbf{u} = (u_1, \dots, u_p) = \mathbf{G}_R(\mathbf{x})$	Realization of \mathbf{U} , with components $u_d = G_d(x_d \mathbf{x}_{<d})$
$\mathbf{x}_{<d} = (x_1, \dots, x_{d-1})$	First $d - 1$ components of \mathbf{x}
$\mathbf{u}_{<d} = (u_1, \dots, u_{d-1})$	First $d - 1$ components of \mathbf{u}
$d(\mathbf{u}), \hat{d}(\mathbf{u})$	Likelihood ratio and its estimate
$T_{j_d}[G_d(x_d \mathbf{x}_{<d})] = T_{j_d}(u_d)$	j_d^{th} normalized shifted Legendre polynomial in $L^2(G_d)$ and $[0, 1]$
$T_k[\mathbf{G}_R(\mathbf{x})] = T_k(\mathbf{u})$	Tensor product of T_{j_d} functions with $k \in \mathcal{K}$, in $L^2(G)$ and $[0, 1]^p$
\mathcal{K}	sets of p -tuple $\{j_1 \dots j_p\}$, $\sum_d j_d \neq 0, j_d = 0, \dots, m_d$
$ \mathcal{K} = M$	Cardinality of \mathcal{K}
$\mathbf{T}(\mathbf{u}) = \mathbf{T}[\mathbf{G}_R(\mathbf{x})]$	$M \times 1$ vector of components $T_k(\mathbf{u}) = T_k[\mathbf{G}_R(\mathbf{x})]$
$\boldsymbol{\theta}$	$M \times 1$ vector collecting the coefficients θ_k
$\hat{\boldsymbol{\theta}}$	$M \times 1$ vector collecting the estimates $\hat{\theta}_k$
D	Deviance statistics

Table 5: A summary of the main notation used throughout the paper.

Supplementary Material

The folder *Codes_and_data* collects the data used in Section 6 and the codes used for the analyses in Figures 1, 2, and 4. The interested reader is directed to the supplementary file *Codes_description.pdf* for a more detailed description of all the codes and files available. The file *Supplement_iGOF.pdf* collects the technical proofs and additional results related to Example I.

Acknowledgments

The author thanks sincerely Estate V. Khmaladze, G. Jogesh Babu and two anonymous referees for the useful discussions and comments. Their valuable feedback has led to a substantial improvement of the quality and clarity of the manuscript.

References

- Adler, R. J. (2000). On excursion sets, tube formulas and maxima of random fields. *Annals of Applied Probability*, pages 1–74.
- Algeri, S. (2019). *TOHM: Testing One Hypothesis Multiple Times*. R package version 1.3.
- Algeri, S. (2020). Detecting new signals under background mismodeling. *Phys. Rev. D*, 101:015003.
- Algeri, S. et al. (2018). Statistical challenges in the search for dark matter. *arXiv:1807.09273*.
- Algeri, S. and van Dyk, D. A. (2020). Testing one hypothesis multiple times: the multidimensional case. *Journal of Computational and Graphical Statistics*, 29(2):358–371.
- Algeri, S. and Zhang, X. (2020). Exhaustive goodness-of-fit via smoothed inference and graphics. *arXiv preprint arXiv:2005.13011*.
- Aprile, E., Aalbers, J., Agostini, F., Alfonsi, M., Amaro, F., Anthony, M., Arneodo, F., Barrow, P., Baudis, L., Bauermeister, B., et al. (2017). First dark matter search results from the xenon1t experiment. *Physical review letters*, 119(18):181301.
- Atwood et al., W. B. (2009). The large area telescope on the fermi gamma-ray space telescope mission. *The Astrophysical Journal*, 697(2):1071.
- Babu, G. J. and Rao, C. R. (2004). Goodness-of-fit tests when parameters are estimated. *Sankhya*, 66(1):63–74.
- Balázs, C. et al. (2017). Colliderbit: a gambit module for the calculation of high-energy collider observables and likelihoods. *The European Physical Journal C*, 77(11):795.

- Barton, D. E. (1953). On neyman’s smooth test of goodness of fit and its power with respect to a particular system of alternatives. *Scandinavian Actuarial Journal*, 1953(sup1):24–63.
- Berk, R., Brown, L., Buja, A., Zhang, K., Zhao, L., et al. (2013). Valid post-selection inference. *The Annals of Statistics*, 41(2):802–837.
- Dauncey, P., Kenzie, M., Wardle, N., and Davies, G. (2015). Handling uncertainties in background shapes: the discrete profiling method. *Journal of Instrumentation*, 10(04):P04015.
- Dissmann, J., Brechmann, E. C., Czado, C., and Kurowicka, D. (2013). Selecting and estimating regular vine copulae and application to financial returns. *Computational Statistics & Data Analysis*, 59:52–69.
- Friedman, J., Hastie, T., and Tibshirani, R. (2001). *The elements of statistical learning*, volume 1. Springer series in statistics New York.
- Ledwina, T. (1994). Data-driven version of neyman’s smooth test of fit. *Journal of the American Statistical Association*, 89(427):1000–1005.
- Lyons, L. (2013). Discovering the Significance of 5 sigma. *arXiv:1310.1284*.
- Mukhopadhyay, S. (2017). Large-scale mode identification and data-driven sciences. *Electronic Journal of Statistics*, 11(1):215–240.
- Mukhopadhyay, S. and Wang, K. (2020). Nonparametric high-dimensional k-sample comparison. *Biometrika (to appear)*.
- Nagler, T., Schellhase, C., and Czado, C. (2017). Nonparametric estimation of simplified vine copula models: comparison of methods. *Dependence Modeling*, 5(1):99–120.
- Nelder, J. (1977). A reformulation of linear models. *Journal of the Royal Statistical Society: Series A (General)*, 140(1):48–63.
- Nelsen, R. B. (2007). *An introduction to copulas*. Springer Science & Business Media.
- Neyman, J. (1937). Smooth test for goodness of fit. *Scandinavian Actuarial Journal*, 1937(3-4):149–199.
- Panagiotelis, A., Czado, C., Joe, H., and Stöber, J. (2017). Model selection for discrete regular vine copulas. *Computational Statistics & Data Analysis*, 106:138–152.
- Parzen, E. (2004). Quantile probability and statistical data modeling. *Statistical Science*, 19(4):652–662.
- Pearson, E. S. (1938). The probability integral transformation for testing goodness of fit and combining independent tests of significance. *Biometrika*, 30(1/2):134–148.
- Priel, N., Rauch, L., Landsman, H., Manfredini, A., and Budnik, R. (2017). A model independent safeguard against background mismodeling for statistical inference. *Journal of Cosmology and Astroparticle Physics*, 2017(05):013.
- Rayner, J. C. W. and Best, D. J. (1990). Smooth tests of goodness of fit: an overview. *International Statistical Review/Revue Internationale de Statistique*, pages 9–17.
- Reed, M. and Simon, B. (1980). Methods of modern mathematical physics i: functional analysis.
- Rosenblatt, M. (1952). Remarks on a multivariate transformation. *The annals of mathematical statistics*, 23(3):470–472.
- Scott, P. (2018). Dark matter model comparison. *BIRS Workshop on Dark matter model comparison, DM-Stat: Statistical Challenges in the Search for Dark Matter*.
- Signoretto, M., Dinh, Q. T., De Lathauwer, L., and Suykens, J. A. (2014). Learning with tensors: a framework based on convex optimization and spectral regularization. *Machine Learning*, 94(3):303–351.
- Taylor, J., Takemura, A., Adler, R. J., et al. (2005). Validity of the expected euler characteristic heuristic. *The Annals of Probability*, 33(4):1362–1396.

- Taylor, J. E. and Worsley, K. J. (2008). Random fields of multivariate test statistics, with applications to shape analysis. *Ann. Statist.*, 36(1):1–27.
- Thas, O. (2010). *Comparing distributions*. Springer.
- Tyson, J. A. (2002). Large synoptic survey telescope: overview. In *Survey and Other Telescope Technologies and Discoveries*, volume 4836, pages 10–20. International Society for Optics and Photonics.
- Westerdale, S. (2016). *A study of nuclear recoil backgrounds in dark matter detectors*. PhD thesis, Princeton University.